Nov 16th, 12:00 AM

Eccentric Connection of Cold-formed Steel Rack Structure

Rokuya Yamasaki

Noboru Yamamoto

Tsunemi Mochinaga

ECCENTRIC CONNECTION OF

COLD-FORMED STEEL RACK STRUCTURE

by

Tokuya Yamasaki,[1] Noboru Yamamoto,[2] Tsunemi Mochinaga[3]

INTRODUCTION

A rack-supported building is designed so that the rack structure will support the roof and side components. Such buildings are widely accepted because of the reduction in total construction costs. For economy and fabrication efficiency, rack frames are composed of thin-wall, cold-formed, steel members assembled with eccentric connections. It is generally believed that such eccentric connections tend to fail locally and to have a bad influence on the buckling strength of the connected members.

In order to evaluate the effect of eccentrically welded connections on the seismic behavior of rack-supported building structural systems, an experimental and analytical investigation was conducted. The study covered the strength and ductility of the connections and the elastic-plastic restoring-force characteristics of rack frames under both static and dynamic loading conditions. The responsive behavior in a full scale shaking-table test was also examined.

Through correlation and estimation of the results, it was determined that eccentric connections provide rack frames with such a large capacity for plastic deformation that rack structures are sufficiently resistant to seismic disturbances and can dissipate the ground motion energy of strong earthquakes.

TEST PROGRAM

During the study, the following tests were carried out to estimate static and dynamic behavior.

1. K-Connection Test: strengths and deformation capacities of the eccentric connections having various distances of eccentricity.
2. Monotonic Loading Tests of Rack Frames: force-deflection relations in the elastic-plastic region of the frames; comparison of the ductility factors of frames assembled by different eccentric connections.
3. Cyclic Loading Tests of Standard Rack Frame: cyclic restoring-force characteristics, failure modes, and high stress fatigue strength of the welded joints in the connections. (The standard frame was selected from the results of tests 1 and 2.)
4. Full Scale Shaking-Table Test: actual acceleration and stress responses to earthquake excitations at intensity levels ranging from 0.1G to 0.5G in maximum acceleration.

[1]General Manager, Structure Research Laboratories, Kawasaki Steel Corporation, Japan
[2]Senior Research Engineer, Structure Research Laboratories, Kawasaki Steel Corporation, Japan
[3]Executive Advisor, Kawatetsu Interlake, Inc., Japan

The specimens and models for these tests were composed of standard, light gage, steel members and fabricated in accordance with standard design drawings except for the distances of eccentricity in the connections (one of the experimental parameters). Two kinds of structural steel sheets specified as JIS SS41 and SAPH45 were used for forming brace and column members respectively. Mechanical properties, such as yield stress and tensile strength, were tested in advance of the structural tests. The results of the coupon tests are presented in Table 1.

K-CONNECTION TESTS

Test Specimens and Procedure

Three types of specimens were prepared for the tests. They had different distances of eccentricity; g = 1.18 in. (30mm), 1.97 in. (50mm), 3.94 in. (100mm) = distance between both braces measured on the column surface, as shown in Figure 1, which also illustrates the method of loading and measurement. The ends of one brace and column were pin-connected to the reaction frame, and, tensile loads were applied in the axial direction at the end of another with a hydraulic jack.

Loads and displacements at appropriate points were measured with a load cell and dial gages respectively.

Test Results and Evaluation

The test results are summarized in Table 2. The behavior of the connection varies widely according to the distance of eccentricity (g) as shown in Figure 2. This figure illustrates the relationship between the axial force and axial displacement of the brace. This includes the elastic shrinkage of the brace and elastic-plastic bending deformation of the column lips in the connection as measured by the dial gages, DG 2 and DG 4, in Figure 1.

The deformation capacity of the K-1 specimen is very small, because local buckling of the unstiffened webs of the compression brace occurs near the connection before visible lip deformation of the column takes place. In the K-2 and K-3 connection tests, deformation of the column lips develops in advance of the local buckling of the braces. Therefore, the deformation capacities of both connections are much larger than the K-1 specimen. In comparing the deformation capacities of the latter two specimens, it is seen that the K-3 specimen has more ability to deform, even though its maximum strength is a little lower than the K-2 specimen.

From both observation of actual behavior and examination of strain values, the basis for the above result is as follows: The longer the eccentric distance is, the more freely the column lips can deform without reciprocal restraint of the adjacent brace ends. Local bending occasioned by eccentricity can be absorbed into the lip deformation, therefore, it is more difficult for the brace to buckle locally. As a result, a larger axial displacement of the brace end can be allowed.

It is obvious that the most suitable connection for an aseismic rack design would be the one that has the largest capacity for deformation. A reliable conclusion, however, has to be based on an analysis of the frame tests.

MONOTONIC LOADING TESTS OF RACK FRAME

Test Models and Procedure

Two types of models were fabricated for the test. All dimensions of the two models were the same except for the distance of eccentricity in the brace-to-column connections as indicated in Figure 3. These distances were 1.97 in. (50mm) for the Model A-M and 3.94 in. (100mm) for the model B-M. These corresponded to specimens K-2 and K-3 in the connection tests respectively.

Figure 4 illustrates the test setup. The lower column was simply supported at each end on a wide flange beam. The test load was applied vertically to the center of the upper column with a hydraulic jack. The lateral supports, which allowed in-plane movement, were attached to each end of the upper column in order to restrain out-of-plane displacement. The bending moments and axial force in each member were measured by means of strain gages. The gages were mounted on the walls of the member at both ends of the section (see Fig. 3) 4.7 in. (119.38mm) from the weld lines. Furthermore, some strain gages were installed on the surfaces of the column lip in the brace-to-column connection to trace bending deformation of the lips. Dial gages were located at appropriate points of the frame to measure the entire deformation.

The compressive load was applied in step-by-step increments. Instrumental measurements were made at each stage, and visual observations were recorded.

Test Results

The load-deflection (P-δ) relationships of models A-M and B-M are shown in Figures 5 and 6 respectively. The shapes of the two P-δ curves apparently vary according to the distance of eccentricity of the brace-to-column connection. In the A-M type test, the gradient of the initial elastic curve decreased because of an increase of deflection after a load of 11.0 kips (49 kN) was attained. At a load of 15.8 kips (70.4 kN), a torsional-flexural buckling of the brace occurred, and, thereafter, the load carrying capacity decreased rapidly. There was no visible deformation of the lips in the connections before the buckling started.

The model B-M showed more ductile behavior than the A-M. After the load exceeded about 14.3 kips (63.7 kN), local bending deformation of the column lips in the brace-to-column connections developed gradually. In this stage, the increment of the load was small, and the deflection grew large without buckling of the braces. Ultimately, the growth of local deformation of the unstiffened webs of the brace ends gave rise to the torsional-flexural buckling of the compressive braces.

As summarized in Table 3, the model B-M is superior to the A-M in deformation capacity, even though the maximum load carrying capacity is somewhat lower.

CYCLIC LOADING TESTS OF RACK FRAME

Test Models and Procedure

The test results described above can easily lead to the conclusion that the standard rack frame should be designed so that it will have a 3.94 in. (100mm) distance of eccentricity in the brace-to-column connections. Two standard rack frame models having the same dimensions as the model B-M in the monotonic loading test were prepared for cyclic loading tests. One of the two models was tested under progressively increasing cyclically-applied deflections simulating earthquake loads. The other model was subjected to a number of large cyclic deflections with constant amplitudes increasing stepwise. The former and the latter models were named B-C and B-F respectively. The experimental setup and measuring instrumentation were the same as in the monotonic test except that an electrical displacement transducer was used in order to record the central deflection of the model B-F.

In both tests, the prescribed cyclic deflections were imposed in a quasi-static manner, and the displacements and strains were measured in appropriate deflection stages. In addition, special attention was paid to the detection of fatigue cracks in the welds of the brace-to-column connections.

Test Results

The cyclic load-deflection relationship of model B-C is shown in Figure 7. Buckling of the brace member occurred under a compressive load (the load sign is plus) in the 8th cycle. After the brace buckled, the load carrying capacity for compressive loads decreased to 60% of what it was before the buckling, whereas the model presented fairly stable hysteretic loops and, in fact, a remarkable increase in deformation capacity for tensile loads.

The result of the model B-F test shown in Figure 8 reveals that the hysteretic loops were stable throughout the test. In addition, there were no cracks observed in the welded connections nor local deformation failure in the member elements.

EVALUATION OF STATIC TEST RESULTS

Fixing Conditions of Brace Ends

Numerical computer analyses of the elastic behavior of models A-M and B-M were performed. An applied program, "FRAME", developed by Japan Univac, Inc. was used to compute the static and dynamic behavior of the frames on the basis of infinitesimal elastic deformation theory.

The analytical models were made on the following assumptions:

1. Members are rigidly jointed at each end.
2. Elastic deformation behavior of the column lips is simulated by an elastic spring deformable only in the direction of brace axis. The spring constants for models A-M and B-M correspond respectively to the elastic slopes of the axial force-deformation curves of specimens K-2 and K-3 in the connection tests.

The elastic load-deflection relationships obtained from the analyses were compared with the test results in Figures 5 and 6. Because each computed relation was in good agreement with the corresponding test result, it proved that the analytical models are appropriate and, especially, that the elastic spring based on the connection tests is an efficient model for evaluating the effect of the column lips on brace end conditions.

Figure 9 shows computed member forces in comparison with measured values for the model B-M. In the case of the axial member forces (Fig. 9a), a good coincidence exists between the analytical and measured values. Measured bending moments at the brace ends, however, are much smaller than the computed results. It points out the fact that the end condition of the braces is considered approximately rotation free because of the flexibility of the column lips. But such an end condition has little influence on the prediction of total elastic behavior as indicated in the comparison of the load-deflection relations occasioned by the characteristics of a truss structure. Nevertheless, it could be assumed that it exerts considerable influence on the brace-buckling load.

The load at which the compressive brace elastically buckles in tortional-flexural mode can be calculated by using the following equation:

$$P_{cr} = \frac{P_w + P_x - \sqrt{(P_w - P_x)^2 + 4\left(\frac{x_o}{r_o}\right)^2 P_w P_x}}{2\left\{1 - \left(\frac{x_o}{r_o}\right)^2\right\}} \tag{1}$$

In Eq. (1) P_x and P_w are the Euler flexural buckling loads about the x axis and the torsional buckling load about the z axis respectively:

$$P_x = \frac{\pi^2 EI}{\ell^2} \tag{2}$$

$$P_w = \frac{1}{r_o^2}\left(C_t + C_w \frac{\pi^2}{\ell^2}\right) \tag{3}$$

in which
- x_o = x coordinate of the shear center (the x axis coincides with the axis of symmetry of the singly symmetric brace section)
- r_o = polar radius of gyration of the cross section about a shear center
- I_x = moment of inertia about the x axis
- E = modulus of elasticity
- ℓ = length of brace
- C_t = torsional rigidity
- C_w = warping rigidity.

The loads calculated from the above equations are indicated in Figures 5 and 6 for models A-M and B-M respectively. The predicted load for brace buckling coincides precisely with the test result of model A-M. In the case of the B-M, however, the predicted load is higher than the test result, because plastic deformation in the column lips precedes the elastic buckling of the brace.

The end condition of the brace, assumed in the calculation as rotation free both in-plane and out-of-plane, proved to be suitable for the prediction of brace buckling just in case there was no plastic deformation in the column lips.

Limit Design Load Dependent on Deformation Capacity

In the Japanese seismic design code, two phases of the design methods are required for comparatively large scale buildings. The first phase is an allowable stress design, and the second phase is a limit load design. The former and the latter are called the Primary Design and the Secondary Design respectively. The purpose of the Secondary Design is to estimate seismic safety of structures according to their capacity for horizontal plastic deformation in the strongest earthquakes. The principle of Secondary Design can be described as

$$ {}_{p}Q_{r} = {}_{e}Q_{r} \cdot D_{s} \tag{4} $$

in which ${}_{p}Q_{r}$ = required maximum horizontal strength of the structure
${}_{e}Q_{r}$ = horizontal force that a structure would be subjected to if it responds elastically to a strong earthquake (corresponding to the response acceleration 1G)
D_{s} = reduction factor depending on the inelastic deformation capacity of the structure ($D_{s} \leq 1$)

The larger the capacity, the smaller the D_{s} value becomes. A value of D_{s} can be calculated with a modified Newmark's[2] potential energy formula as follows:

$$ D_{s} = \frac{D_{h}}{\sqrt{2\mu - 1}} \tag{5} $$

in which $D_{h} = 1.5/(1 + 10\,h)$
μ = ductility factor
h = damping ratio.

By substituting the results of the frame tests for μ and 0.03 for h, one finds that Eq. (5) gives the D_{s} values of 0.66 and 0.46 for models A-M and B-M respectively.

On the basis of design specifications in the seismic code of Japan, the maximum strengths required for the lowest level of the rack frames can be estimated for both models. In this estimation, the above D_{s} values are used, and the same worst condition of foundations is assumed. The estimated results are indicated in Figures 5 and 6 together with the Primary Design loads. If one compares the required maximum strengths (${}_{r}P_{m}$) to the experimental maximum strengths (${}_{e}P_{m}$), one finds that model B-M obviously has a greater safety allowance than model A-M. That is,

$$\frac{e^P_m}{r^P_m} \approx 1.0 \qquad \text{for model A-M}$$

and

$$\frac{e^P_m}{r^P_m} = 1.35 \qquad \text{for model B-M.}$$

It is apparent that the difference in the safety allowance between the two models depends entirely on the deformation capacity they possess.

Cumulative Damage During Strong Earthquakes

Earthquake response has been used to analyze cumulative plastic deflections in order to verify seismic safety. In the analyses, the modified cyclic force-deflection (P-δ) relation[3] is derived from the idealized monotonic approximation as illustrated in Figure 10 on the basis of the experimental P-δ relation of the standard frame (model B-M).

A six degree-of-freedom system, composed of six masses and shear springs corresponding to six levels of live load locations, can be used for the analyses as a mathematical model. The shear springs act in accordance with the cyclic, lateral load-displacement relation as indicated above. In addition, they include the effect of axial deformation of the columns in the elastic region. The input constants are mainly: mass weight = 2.2 kips (9.8 kN), maximum acceleration = 0.34 G, and damping ratio = 0.03. The analyses were conducted for two kinds of actual acceleration records of well-known earthquakes: (El Centro 1940 NS and Taft 1952 EW) with the Runge-Kutta integration method.

According to the computed results, the floor displacement of the lowest level has the largest value of all the other floors throughout the duration of an earthquake. Computed story shear-displacement histories of the lowest level are shown in Figure 11. In this figure, some of elastic paths have been omitted for simplicity. The cumulative plastic displacement, δ_t, of a story in one direction can be calculated by

$$\delta_t = \Sigma \delta_{pi}, \tag{6}$$

in which δ_{pi} is the plastic displacement in ith cycle in the same direction as δ_t.

The value of δ_t can be compared to the maximum failure displacement, δ_B, in the monotonic loading condition as follows:[3]

δ_t = 0.59 in. (14.9mm) < δ_B = 0.83 in. (21.2mm) for the El Centro earthquake
δ_t = 0.44 in. (11.3mm) < δ_B = 0.83 in. (21.2mm) for the Taft earthquake

It has been proven that the cumulative plastic displacement never reaches the critical displacement value during such strong earthquakes as the El Centro or Taft.

Cyclic Restoring Force Characteristics and Fatigue in Welded Connections

The cyclic behavior of the standard rack frame retained stable loops throughout the test as shown in Figure 7 for model B-C. This confirms the fact that there is no abrupt decrease in the restoring force under fluctuating earthquake loads.

The result of the low cycle fatigue test that is shown in Figure 8 shows no sign of cracks or fractures in the welds of the brace-to-column connections. In addition, strain amplitudes measured on the lip surfaces adjacent to the welds are plotted against the number of cycles in Figure 12. In this figure, the plastic strain amplitude maintains a constant value through constant deflection cycles; therefore, no indication of the fatigue fracture can be found. The fatigue safety was also verified by observing the welds throughout the tests.

FULL-SCALE SHAKING-TABLE TESTS

Test Model and Procedure

The test model consisted of two units of 29.8 (9m) foot-high standard rack frames as illustrated in Figure 13. The support rails were connected to the frames at a total of six levels in the upward direction to support live loads on wooden pallets. A unit of 2.2 kips live load was prepared by piling steel plates in a steel box. These steel plates and the box were welded to each other to prevent mutual movement. Each column was anchored to the shaking-table by two 0.787 in. (20mm) D bolts. The size of the shaking-table and other capacities of the electromagnetic vibration testing machine are summarized in Table 4.

Pairs of strain gages were installed on the symmetrical surfaces of key members to measure axial member stresses. The locations and measuring directions of the accelerometers are shown in Figure 13. Displacements could be measured through the same accelerometers by means of an analog-type double-integrator in real time. In Figure 13, the locations of the accelerometers marked (1) $\sim$ (6) correspond to the six lumped masses in the model for the response analysis described later. The other accelerometers installed at locations F2, F4, and F6 were used to measure accelerations of the frame at the same levels as the live loads, and the accelerometers at L2, L4, and L6 were used to register the acceleration responses of the live loads. It should be noted that a "story" is assigned to the lumped mass levels (1) $\sim$ (6), whereas the "level" is assigned to the live load levels F2, F4, L2, etc. In addition to the instrumental measurements, relative movements between the live load boxes and the pallets as well as between the pallets and the support rails were observed. These were determined by reading the distances that the boxes or the pallets slid during each forced excitation stage.

Results of Free Vibration Test, Frequency Sweep Test

The pull-back method was adopted for the free vibration test. An initial displacement of 0.2 in. (5mm) was imposed on the top of the frame. Data related to acceleration and displacement were recorded twice. The natural frequency and damping ratio derived from the test are shown in Table 5.

The frequency sweep test involves the application of steady-state sinusoidal excitation and is conducted by varying the frequency progressively in successive steps. At each frequency step, the measurement was repeated. As a result, the measured amplitudes of motion of the frame were plotted against the exciting frequencies, and from these the resonance curves were drawn as shown in Figure 14. The natural periods for the first

three modes derived from the resonance curves are indicated in Table 6. These natural periods were compared with the ones from the dynamic analysis in order to examine the applicability of an analytical model.

Results of Earthquake Excitation Tests

A series of ten shaking tests were conducted. The excitation of the shaking table simulated the actual ground motion recorded by accelerograms during the 1940 El Centro NS earthquake. The maximum acceleration produced in the shaking table for each duration of excitation was increased progressively as the test series proceeded. The maximum acceleration at the final test was 0.5G as shown in Table 7.

Measured values of the maximum acceleration responses of both the frame and the live load at each level are listed in Table 7, which covers the entire test series. These responses are plotted against the table accelerations in Figure 15. Furthermore, Figure 16 shows distributions of the maximum response acceleration along the frame height for the No. 5 and No. 7 tests. It is obvious in Figure 15 that the response values themselves, together with the increasing rates of the responses against input accelerations, are not so high as ordinarily observed in steel structures. For the 6th level, in particular, the acceleration of the live load stops increasing in spite of the continuous increase of the frame response to the table accelerations in the range over 0.35 G.

Special attention should be paid to the fact that the stress in every member was in the elastic range even during the strongest excitation of the No. 10 test. Thus, from the measured elastic stresses, the story shears could be calculated and plotted against the maximum table accelerations in Figure 17. Figure 18 also shows the story shears from the viewpoint of variation with story height. Besides this, the maximum axial force in the column is related to story heights as shown in Figure 19.

The above test results reveal that the maximum responses in both acceleration and member stress are much lower as a whole than expected for normal responses, despite the adequate value of the damping ratio (see Table 5). This is ascribed to the fact that the reciprocal transmission of forces between the frame and the live load is incomplete because of the pallet slide on the support rail. In fact, a slide of 0.08 to 0.12 in. (2.0 to 3.1mm) was observed after each excitation of input acceleration in the range over 0.3 G.

EVALUATION OF DYNAMIC TEST RESULTS

Dynamic Response Analysis

The same type of program "FRAME" that was used in the static analyses was used for the dynamic analysis. In addition to the assumptions that were made in the "Fixing Condition of Brace Ends", the test model was idealized into a mathematical plane frame model, which consisted of 59 members connected by 42 grids including support rails as illustrated in Figure 20. Both the dead load of the frame and the live loads were distributed among the six lumped masses. It should be noticed that the mass in the analytical model was completely fixed to the frame.

The input acceleration data for the analysis were digitized. These were converted from the table motion analog records of tests Nos. 5, 7, and 10. The conversions were executed at an interval of 0.01 second. The integration method used in the computation was a linear acceleration method applied in a time interval of 0.01 second. The assumed damping ratio of 2.5% was obtained from the free vibration test.

Comparison Between Analysis and Tests

Computed vibration modes are illustrated in Figure 21 for the first three modes. The natural frequencies obtained from the analysis agree well with the resonance test result as indicated in Table 6. Hence, the analytical model proved to be suitable for an interpretation of the dynamic behavior of the rack frame.

Figures 15 and 16 show that the maximum accelerations at the fourth and sixth levels in the tests are one-half to one-third as low as the computed values. Similarly, the story shears of the test results are much smaller than the computed values, and this tendency is prominent at the lower stories as indicated in Figures 17 and 18. When comparing the ratios of the experimental story shears to the analytical values, one finds that these are 25% at the third story and 17% at the first story. In contrast to this, the measured axial forces in the column are no more than 35% at the third story and 40% at the first story of the computed axial forces as shown in Figure 19. Therefore, the column is sustaining more load in actual response than braces comparatively because of the predominant bending deformation that is likely to occur in slender cantilevered structures.

The results of the above comparison are ascribed to the fact that the higher the actual acceleration response is, the easier a live load can slide on support rails. Consequently, the effective mass to actual strong earthquakes can be estimated at a conservative 30% of net values for story shears and 40% of those for column axial forces.

It can be concluded that the earthquake design load in the current code is unfairly large in the absence of the corresponding actual dynamic behavior of such a structural system. In the near future, these research achievements will be included in seismic design calculations based on the collection of more detailed related data.

CONCLUSIONS

For the eccentric brace-to-column connection in which the centroids of the sections do not intersect at one point, the connection can allow for a greater capacity of elastic-plastic deformation as the distance of eccentricity increases. Hence, in accordance with the test results, the most suitable distance of eccentricity can be selected for the standard rack frame so as to produce a greater capacity of seismic energy dissipation.

In the standard rack frame, a large relative displacement between adjacent connections of a brace is permitted, because the column lips in the connection deform plastically before the brace buckles. The entire rack frame is thus capable of large lateral displacements or has a great energy dissipation capacity against destructive earthquakes. The lips of the columns, nevertheless, remain in a materially elastic region for the load specified by the allowable stress design.

The cyclic loading tests indicate that the cyclic load-deflection relation of the frame draws stable hysteretic loops even after brace buckling, and that cracks or fractures occasioned by high strain fatigue do not occur in the welded connections between braces and columns.

The shaking-table tests revealed that actual responses of the rack system are considerably lower than theoretical predictions. This is because of the slides of pallets on support rails. In fact, the maximum story shear and axial force in columns are no more than 30 and 40%, respectively, of the theoretical predictions even on the safe side of the estimates.

The results of this study can contribute to the seismic design of rack-supported buildings.

ACKNOWLEDGMENTS

This research was performed under the technical guidance of Dr. Ben Kato, professor of Tokyo University, for the purpose of getting the Specific Approval of the Minister of Construction of Japan on the standard design of rack-supported buildings. The valuable advice of Roger E. Scholl, vice president of URS/John A. Blume & Associates, Engineers, is appreciated.

APPENDIX I - REFERENCES

1. Column Research Committee of Japan, "Elastic Stability Handbook", Corona Publishing Co., Ltd., Tokyo, Japan, 1969 (in Japanese).
2. Veletsos, A. S., Newmark, N. M., "Effect of Inelastic Behavior on the Response of Simple Systems to Earthquake Motions", Proc. 2nd WCEE, Vol. II, July 1960.
3. Kato, B., Akiyama, H., "Predictable Properties of Structural Steels Subjected to Incremental Cyclic Loading", Preliminary Publication of IABSE Symposium, Lisbon, 1973.

APPENDIX II - NOTATIONS

C_t = torsional rigidity

C_w = warping rigidity

D_s = reduction factor for horizontal design load

E = modulus of elasticity

g = distance of eccentricity

G = acceleration of gravity

h = damping ratio

N = axial force in member

I_x = moment of inertia about x axis

P = load

P_{cr} = torsional-flexural buckling load

P_w = torsional buckling load about z axis

P_x = Euler flexural buckling load about x axis

P_y = yield load

Q = story shear

$_pQ_r$ = required maximum horizontal strength of structure

$_eQ_r$ = horizontal force that structure would be subjected to, if it responds elastically to a strong earthquake

r_o = polar radius of gyration of cross section about shear center

x_o = x coordinate of the shear center

δ = deflection

δ_B = deflection at failure

μ = ductility factor

Table 1 Mechanical Properties of Materials

Steel	Thickness (in.)	Y.P. (ksi)	T.S. (ksi)	El. (%)
SS41	0.13	42.6	63.1	30
SAPH45	0.16	45.1	67.6	33

Table 2 Test Results of Brace-to-Column Connections

Specimen	Yield Strength (kips)	Max. Strength (kips)	Max. Deformation (in.)
K-1	——	9.0	0.03
K-2	9.7	10.8	0.57
K-3	8.7	9.1	0.99

Table 3 Test Results of Rack Frames

Model	Yield Load (kips)	Max. Load (kips)	Max. Deflection (in.)	Ductility Factor
A-M	12.8	15.8	0.46	1.9
B-M	12.8	14.9	1.16	3.6

Table 4 Specification for Electromagnetic Vibration Testing Machine

Loading Capacity	16.5 kips
Frequency Range	0.1 ∿ 50 Hz
Max. Acceleration	0.5 G (Full Load)
Max. Velocity	11.8 in./sec.
Max Displacement	± 2.0 in.
Shaking-Table Size	78.7 x 118.1 in.
Wave Form	Regular & Random
Table Suspension	Hydrostatic Bearing

Note : 1 in. = 25.4 mm
1 ksi = 6.895 MN/m^2
1 kip = 4.448 kN

Table 5 Free Vibration Test Results

Recorded Data	Natural Period (sec.)	Damping Ratio
Acceleration	0.36	0.025
Displacement	0.36	0.022

Table 6 Natural Periods from Frequency Sweep Tests

(unit:sec.)

Mode	Test Result		Computed Result
	Acceleration Response	Displacement Responce	
1st	0.38	0.36	0.34
2nd	0.11	0.11	0.11
3rd	0.067	0.067	0.066

Table 7 Maximum Response Accelerations Observed in Shaking-Table Tests

(unit: G)

Test No.	Table Acceleration	Frame Level			Live Load Level		
		2nd	4th	6th	2nd	4th	6th
1	0.13	0.10	0.10	0.14	0.09	0.12	0.24
2	0.16	0.13	0.13	0.18	0.12	0.15	0.31
3	0.20	0.16	0.16	0.22	0.15	0.18	0.39
4	0.25	0.20	0.19	0.27	0.17	0.22	0.49
5	0.29	0.23	0.22	0.33	0.21	0.26	0.55
6	0.35	0.28	0.28	0.41	0.23	0.29	0.66
7	0.40	0.33	0.33	0.47	0.28	0.35	0.69
8	0.41	0.39	0.35	0.61	0.34	0.40	0.74
9	0.46	0.45	0.46	0.85	0.39	0.46	0.65
10	0.50	0.54	0.57	1.02	0.44	0.53	0.77

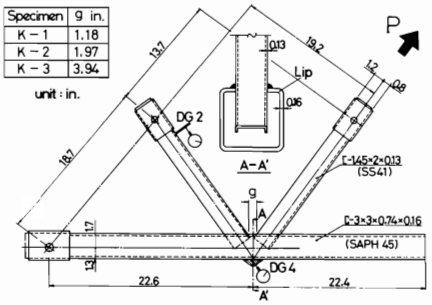

Fig. 1

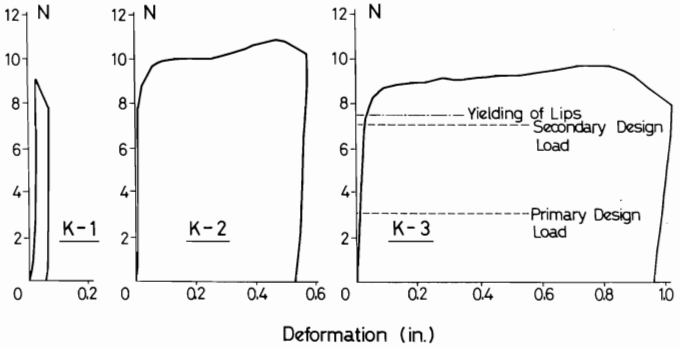

Fig. 2

Type	g	gs	ge
A–M	1.97	0.75	1.22
B–M	3.94	1.81	2.13

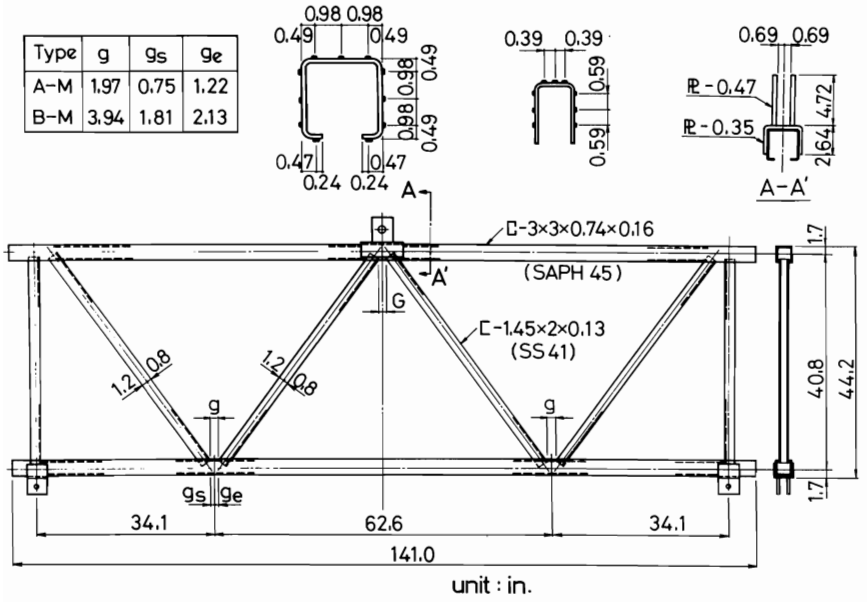

Fig. 3

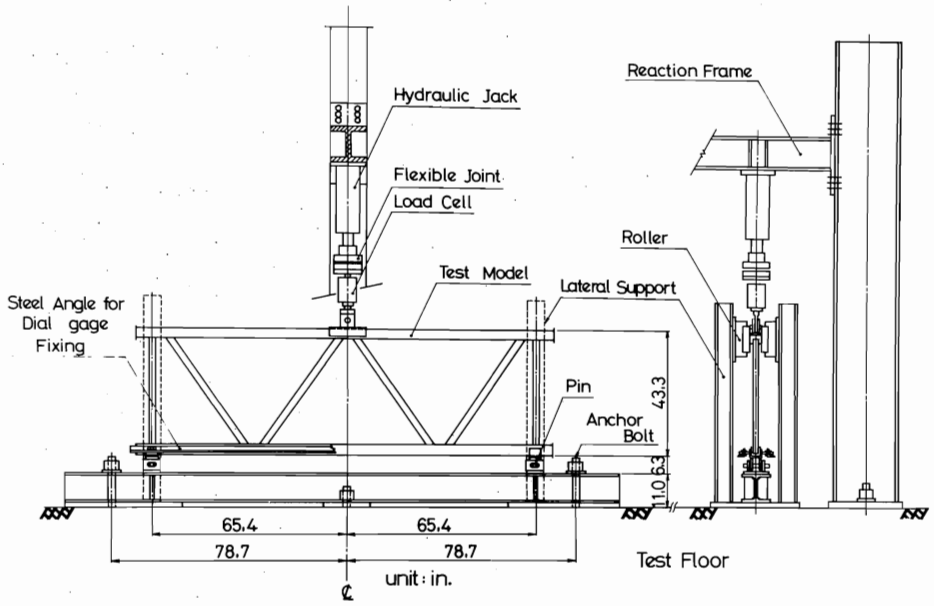
Hydraulic Jack
Flexible Joint
Load Cell
Test Model
Steel Angle for
Dial gage
Fixing
Reaction Frame
Roller
Lateral Support
Pin
Anchor
Bolt
43.3
11.0 6.3
65.4
65.4
78.7
78.7
unit : in.
Test Floor

Fig. 4

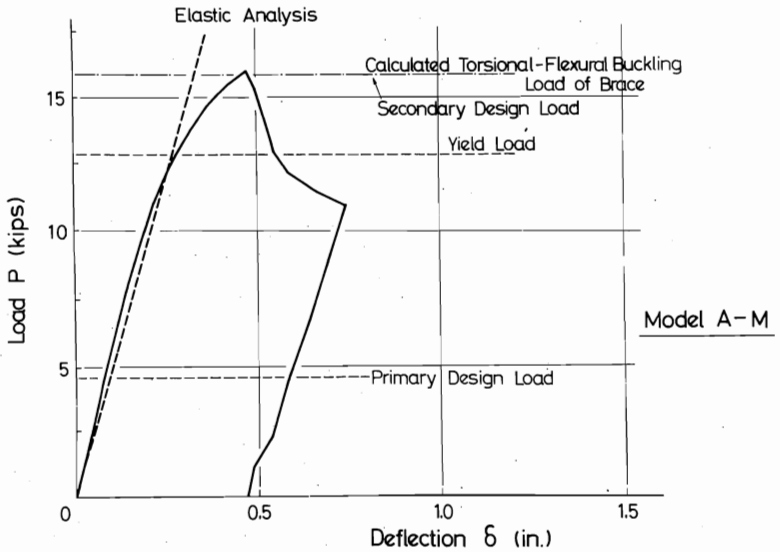
Elastic Analysis
Calculated Torsional-Flexural Buckling
Load of Brace
Secondary Design Load
Yield Load
Primary Design Load
Model A-M
Load P (kips)
15
10
5
0
0.5
1.0
1.5
Deflection δ (in.)

Fig. 5

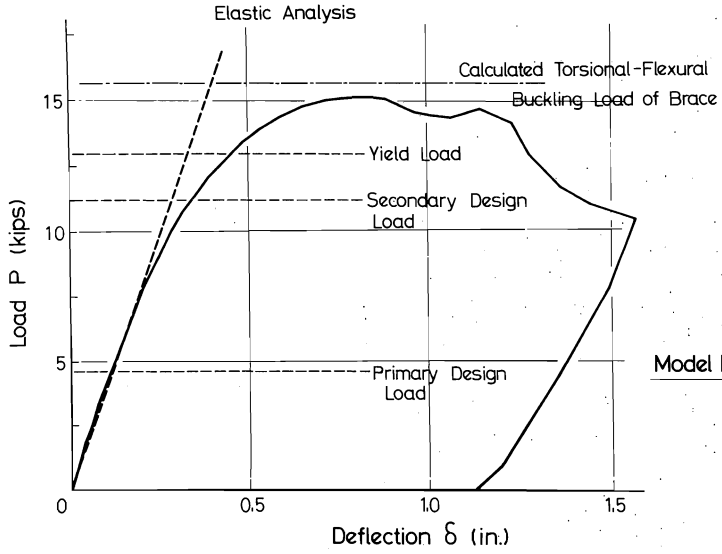

Fig. 6

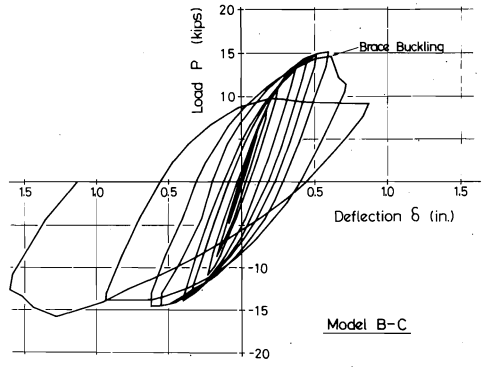

Fig. 7

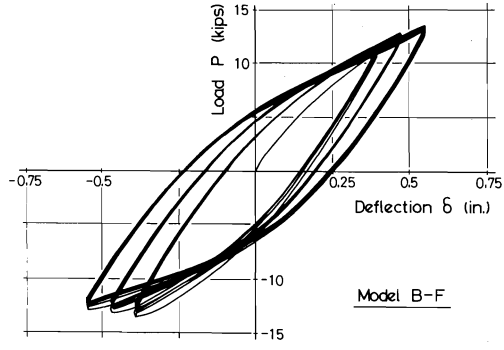

Fig. 8

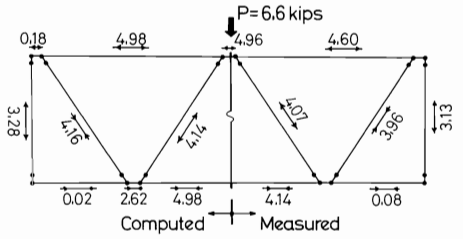

Fig. 9 (a)

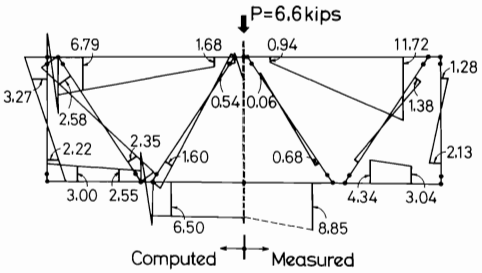

Fig. 9 (b)

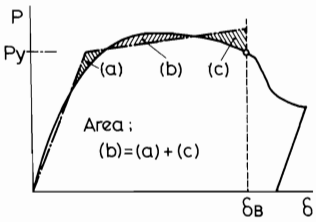

Fig. 10

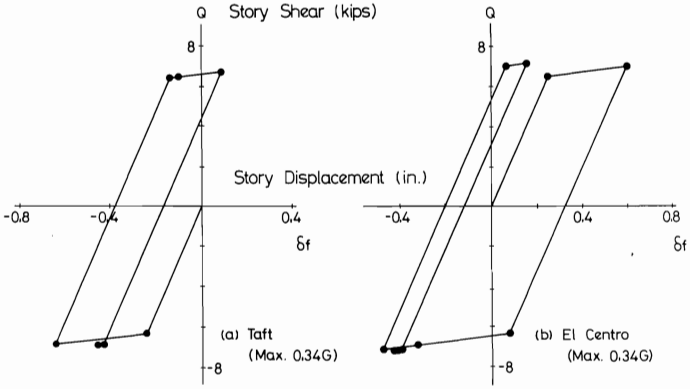

Fig. 11

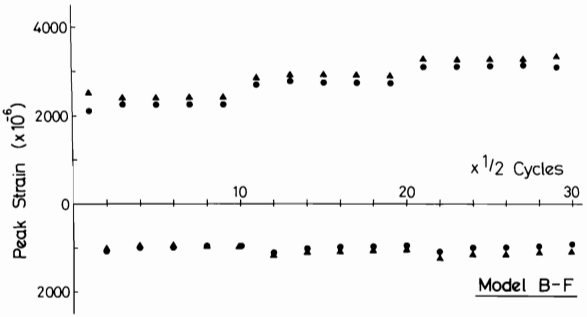

Fig. 12

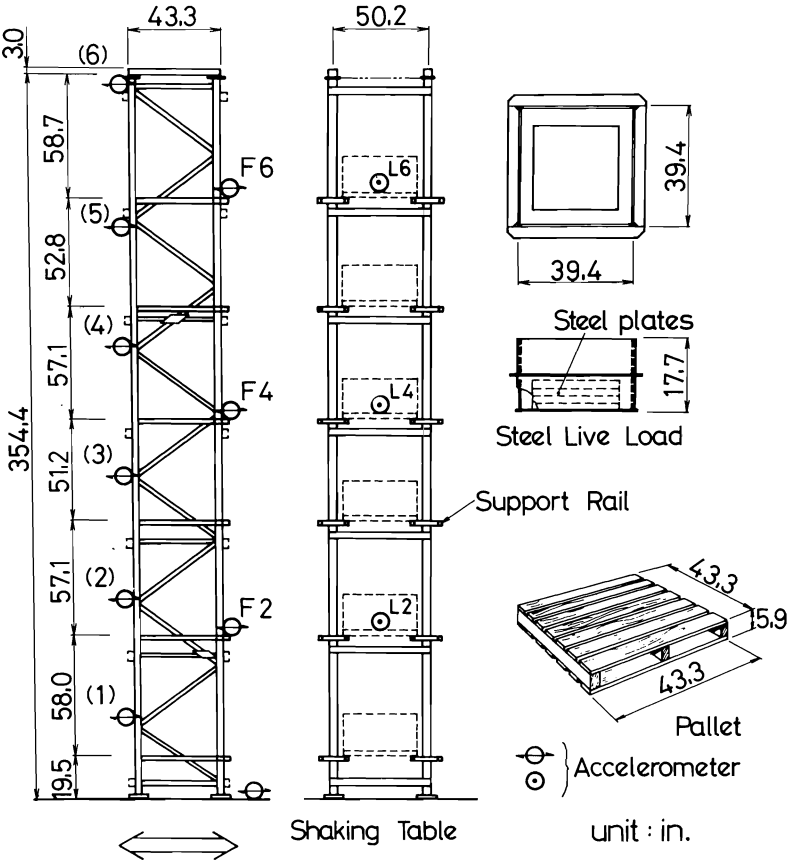
43.3
50.2
3.0
(6)
58.7
F6
L6
(5)
52.8
(4)
57.1
F4
L4
354.4
51.2
(3)
57.1
(2)
F2
L2
58.0
(1)
19.5
39.4
39.4
Steel plates
17.7
Steel Live Load
Support Rail
43.3
15.9
43.3
Pallet
Accelerometer
Shaking Table
unit : in.

Fig. 13

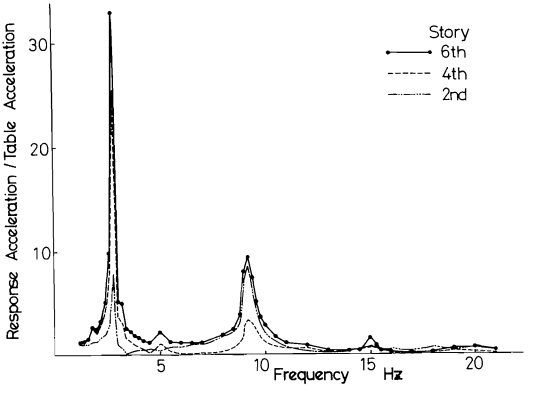
Response Acceleration / Table Acceleration
30
20
10
5
10
15
20
Frequency Hz
Story
6th
4th
2nd

Fig. 14

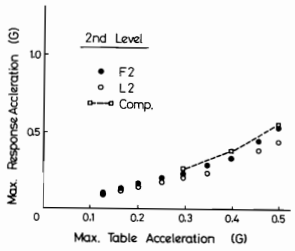

Fig. 15 (a)

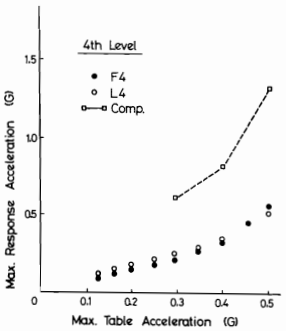

Fig. 15 (b)

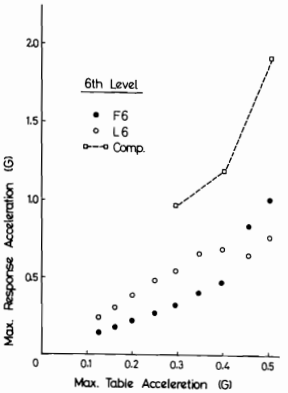

Fig. 15 (c)

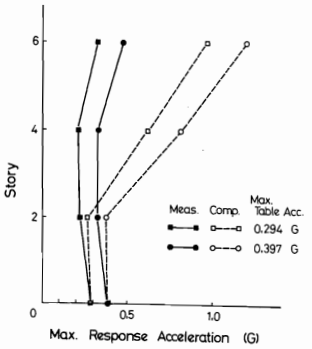

Fig. 16

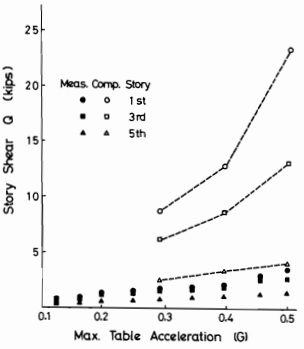

Fig. 17

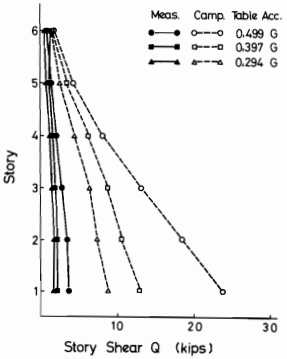

Fig. 18

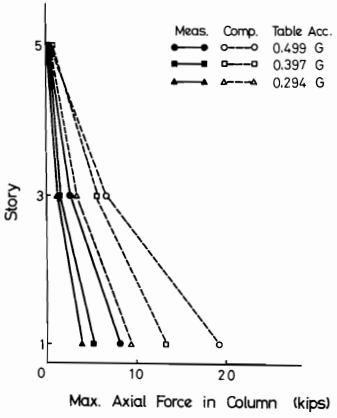

Fig. 19

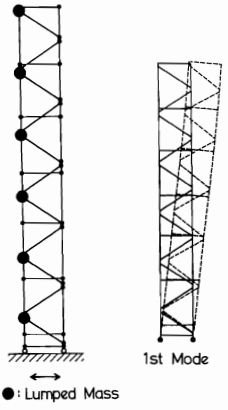

Fig. 20

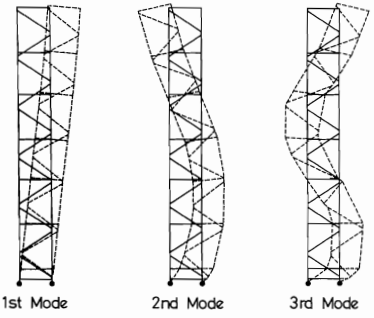

Fig. 21